Supporting Information

An organic-inorganic hybrid Indium molecular ferroelectric originated from "butterfly-flapping" model 1,5-diazabicyclo[3.3.0]octane

Guoyong Chen,[1] Mingjun Zou,[1] Mengxiang Luo,[1] Xiuli You,[2,] Yaozhen Wu,[1] Lin Zhou,[1] Wenjing Guo,[1] Zhenhong Wei,[1,]* Hu Cai[1,3,]**

G. Chen, M. Zou, M. Luo, Y. Wu, L. Zhou, W. Guo, Z. Wei, H. Cai

School of Chemistry and Chemical Engineering Nanchang University, Nanchang City, 330031, P.R. China.

X. You

Jiangxi Provincial Key Laboratory of Organic Functional Molecules; Institute of Organic Chemistry, Jiangxi Science and Technology Normal University, Nanchang, Jiangxi 330031, P.R. China.

H. Cai

State Key Laboratory of Coordination Chemistry, School of Chemistry and Chemical Engineering, Nanjing University, Nanjing 210093, China.

Measurement Methods

Differential scanning calorimetry (DSC), single-crystal X-ray diffraction (SC-XRD), powder X-ray diffraction (PXRD) measurements, dielectric measurements, Second harmonic generation (SHG) measurements, Piezoresponse Force Microscopy (PFM) Measurements and Variable temperature Raman measurements.

Single-Crystal X-ray Crystallography

Suitable-sized usable crystals were obtained by the solvent evaporation method. After selecting appropriate crystals, they were mounted on the HyPix diffractometer of the XtaLAB Synergy R diffractometer (equipped with a DW system). The data were measured using Mo-Kα radiation (λ = 0.71073 Å), and the crystal temperature was kept constant during the data collection process. Detailed parameters are shown in Table S1. The structure was solved by the direct method using the ShelXS [1] structure analysis program, with Olex2 [2] as the graphical interface. Finally, the model was refined by the least squares method using the 2019/3 version of ShelXL 2019/3 [3].

Variable-temperature powder X-ray diffraction (PXRD)

Powder X-ray diffraction (PXRD) data were obtained on a Bruker D8 ADVANCE X-ray diffractometer using Cu Kα radiation (λ = 1.5418 Å) with a temperature-controlled stage (Bruker VT 1000) in the range of 260–400 K under a nitrogen atmosphere. Diffraction patterns were collected in the 2θ range of 5–60° with a step size of 0.02° and a collection time of 10 s per step. Data were processed using Bruker Diffrac.Suite software for background subtraction and Kα1/Kα2 separation, with temperature points optimized to capture phase transitions observed in DSC.

IR measurements

The Fourier transform infrared (FTIR) spectra were obtained using a Bruker Alpha II instrument.

Thermogravimetric analysis

TGA was carried out with a PerkinElmer TGA 8000 at a rate of 20 K min^{-1} in a nitrogen atmosphere. The measurement temperature range was from 300 K to 800 K.

Thermal analyses

Differential scanning calorimetry (DSC) measurements were performed with a NETZSCH DSC 200F3 instrument. Powder samples underwent both heating and cooling processes at a consistent rate of 15 K min^{-1} under aluminum crucibles and nitrogen atmosphere.

SHG measurements

All SHG measurements in this work were performed using the standard Kurtz-Perry method, with a pulsed Nd: YAG laser (LUMIBIRD CFR162401B1) as the excitation source, which outputs a fundamental wavelength of 1064 nm with a pulse width of 11.7 ns and a repetition rate of 10 Hz. The second harmonic signal was detected by a photomultiplier tube (PMT, FJIRSM). The temperature-dependent SHG response of the sample was collected on a variable-temperature stage (UNKAM THMS600) over a temperature range of 220 K to 400 K.

Dielectric measurements

The complex dielectric constant was measured using a DMS-1000 dielectric temperature spectrum measurement system at a testing frequency range of 500 Hz to 1 MHz. Compound 1 was compressed into a pellet under 10 MPa for 1 min using a powder tablet press (Shanghai Sino SYP-40C), yielding a powder pellet sample with a thickness of 1.56 mm. Silver conductive adhesive was coated on both surfaces of the sample, each with an area of 25.6 mm^2, serving as the upper and lower electrodes respectively. A Linkam THMS600 temperature-controlled stage was used to precisely control the sample temperature. Variable-temperature dielectric spectra were collected over a temperature range of 280 K to 370 K, with a heating and cooling rate of 5 $K \cdot min^{-1}$.

Thin-Film Preparation

Indium tin oxide (ITO) conductive glass substrates (1cm×1cm) were ultrasonically cleaned in acetone, anhydrous ethanol, and deionized water for 15 minutes each in sequence. 20 mg of Compound **1** was dissolved in 250 μL ethyl acetate. 50 μL of the solution was dropped onto the ITO substrate, by spin-coating at 3000 rpm for 30 s. After spin-coating, the solvent was allowed to evaporate slowly at room temperature to form a polycrystalline film. Annealing was carried out at 60 °C for 6 hours to remove residual solvent, and the thin film sample was finally obtained. The thickness of the thin film was characterized using an Oxford Instruments Cypher ES AFM, which is equipped with a PFM module for subsequent ferroelectric domain characterization. A partial rectangular region of the thin film was scraped off with a clean surgical blade to fully expose the underlying ITO conductive glass substrate, generating a well-

defined height step. Topographic scanning was then performed in AFM contact mode over a 50 μm × 50 μm area for 3 randomly selected regions containing the step structure on the same sample, and the single-point thickness of the thin film was derived from the height difference of the step. The average thickness of the thin film used for PFM ferroelectric property characterization was finally determined to be 1.32 μm by averaging the values from the 3 test positions.

To verify the phase purity of the as-prepared thin film, XRD measurement was carried out on a Bruker D8 ADVANCE X-ray diffractometer with Cu Kα radiation (λ = 1.5418 Å), with a 2θ scanning range of 5° to 60°. The collected diffraction pattern is in good agreement with the simulated XRD pattern from the single-crystal structure of Compound **1.** (Figure S11), and no additional impurity peaks were detected, fully demonstrating that the as-prepared thin film is phase-pure.

Piezoresponse Force Microscopy (PFM) Measurements

The PFM measurements were conducted using a piezoresponse force microscopy (PFM) system, (the Oxford instrument Cypher ES) with a high-voltage package. We utilized conductive Pt/Ir-coated silicon probes (EFM, Nanoworld) with a nominal spring constant of approximately 2.8 (EFM, Nanoworld) nN/nm and a free-air resonance frequency of roughly 75 kHz. The PFM experiments nN/nm were carried out in Dual Frequency Tracking mode.

Polarization-Electric Field (P-E) Hysteresis Loops

The P-E hysteresis loops measurement was performed on high-quality single crystals of Compound **1**. The selected high-quality crystal has dimensions of a×b×c = 5.275 mm × 0.256 m × 0.750 mm (Determine the crystal axis using Rigaku XtaLAB Synergy DW). Conducting silver paste was coated on the two crystal planes perpendicular to the c-axis to prepare electrodes. Before testing, the sample was dried in a vacuum oven at 30 °C for 60 minutes to ensure good contact between the silver paste and the crystal surface. The P-E hysteresis loops were recorded on a Radiant Precision Premier II ferroelectric test system at room temperature (298 K), using the standard Sawyer-Tower circuit mode. The system is equipped with an Agilent 33500B waveform generator to generate the standard triangular wave excitation signal, a Trek model 609E-6 high voltage waveform amplifier to amplify the excitation signal to the target high voltage range, and a Keithley 6517B electrometer to collect the polarization current signal and convert it into the polarization value of the sample.

Variable temperature Raman measurements

The Raman shifts were measured by the Raman spectrometer (Horiba, LabRAM HR Evolution) with a reflection method. The excitation laser was 633 nm. 50× microscope objectives were used to focus the excitation on the micrometer-size samples. The spectrum was dispersed by a 600-groove per millimeter diffraction grating and accumulated 3 times with an exposing time of 2 s. The temperature range is 260 K – 390 K.

Elemental analysis

Elemental analysis was performed on a Vario EL Cube elemental analyzer (Elementar Analysensysteme GmbH, Hanau, Germany). Approximately 2~3 mg of the crystalline sample was accurately weighed into a tin capsule and combusted at 1150 °C under a dynamic oxygen atmosphere. The contents of C, H, and N were determined by thermal conductivity detection (TCD). Calibration was performed using sulfanilamide as the standard reference material.

Computational modelling.

Dipole moment calculation are carried out within the Gaussian 16 program under different theoretic algorithms (def2-SVP and aug-cc-pVDZ).

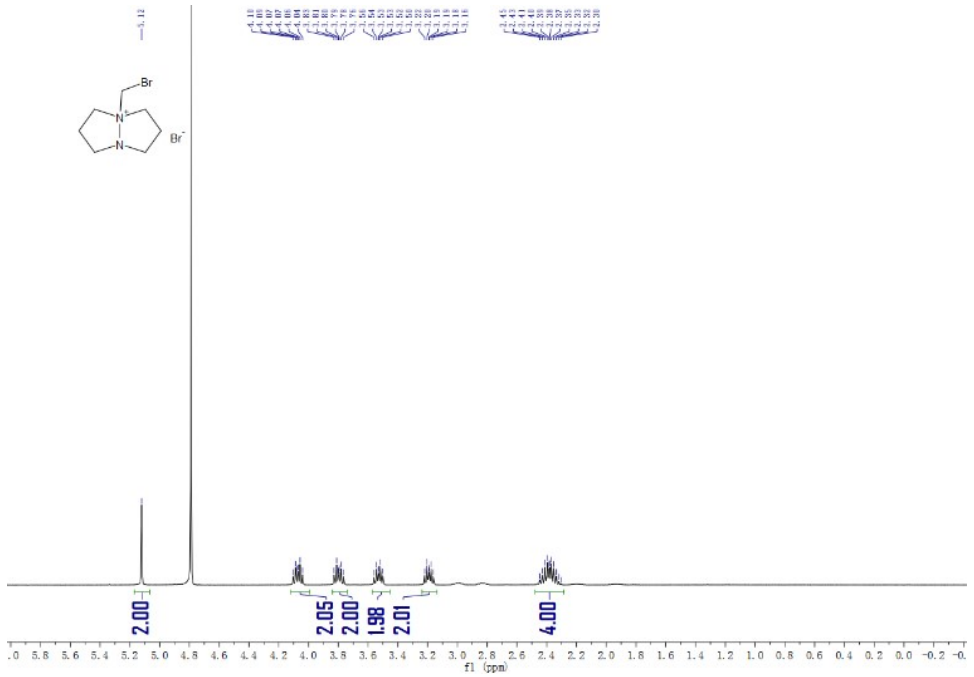

Figure S1. ^{1}H NMR spectrum of [$BrCH_2$-3.3.0-Dabco]Br (400 MHz, D_2O).

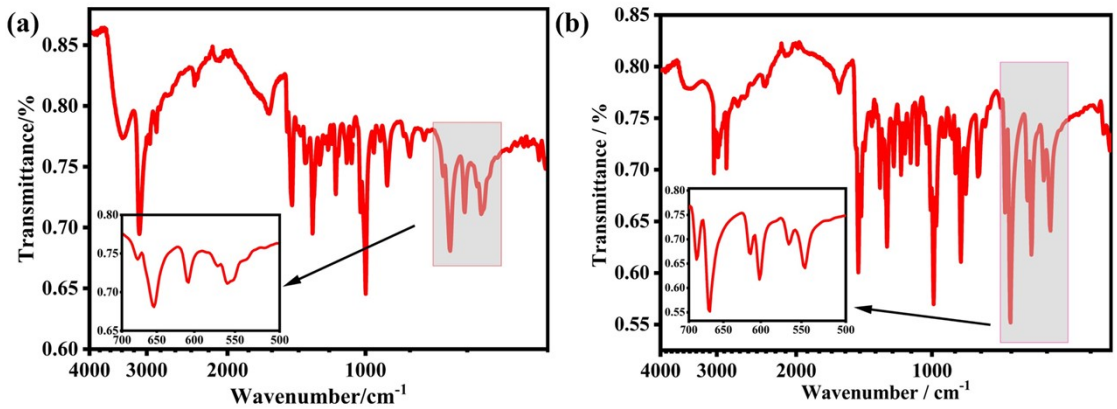

Figure S2. The infrared spectra of compounds (3.3.0-Dabco)[$InBr_4$] (a) and **1** (b).

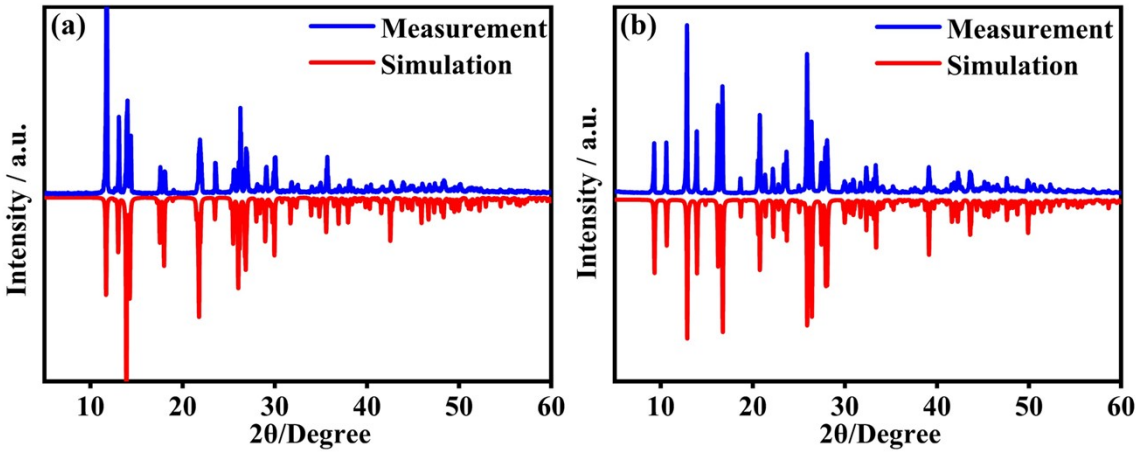

Figure S3. The powder X-ray diffraction measurement results of compounds (3.3.0-Dabco)[$InBr_4$] (a) and **1** (b) at room temperature.

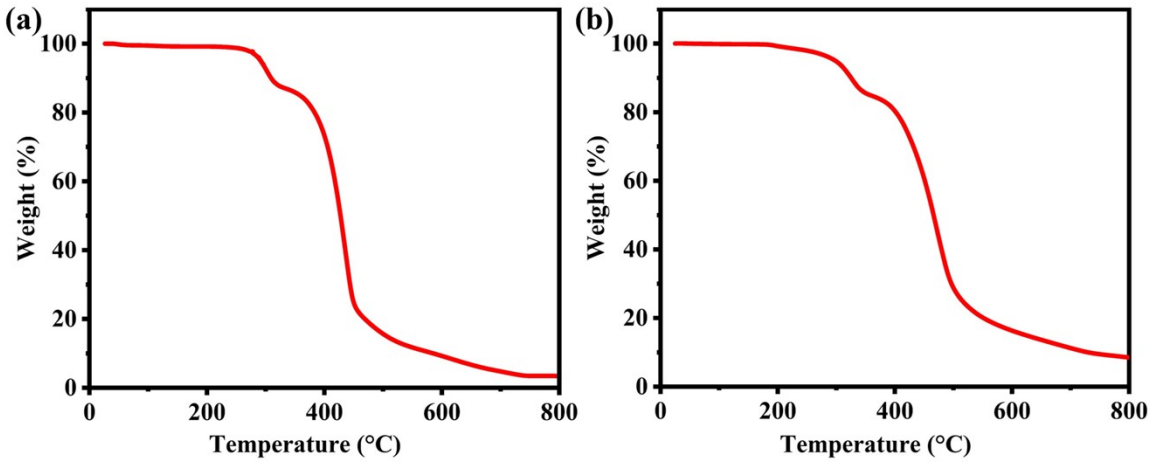

Figure S4. The thermogravimetric analysis of compounds (3.3.0-Dabco)[$InBr_4$] (a) and **1** (b).

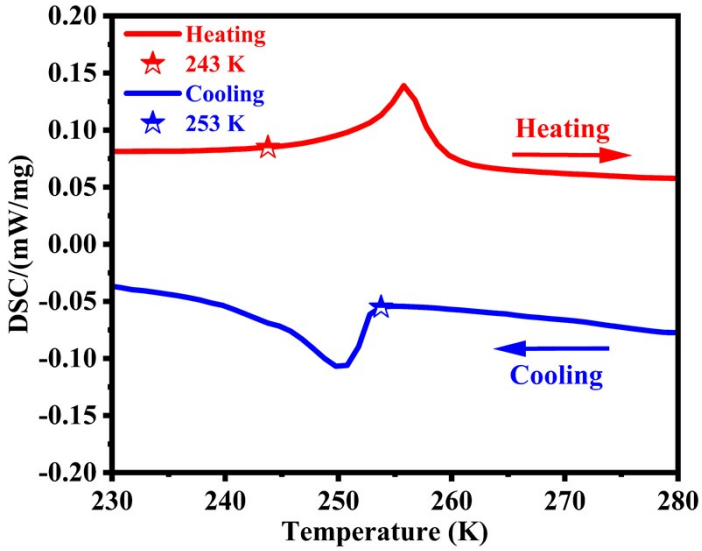

Figure S5. The DSC curves of compound (3.3.0-Dabco)[$InBr_4$] upon heating and cooling.

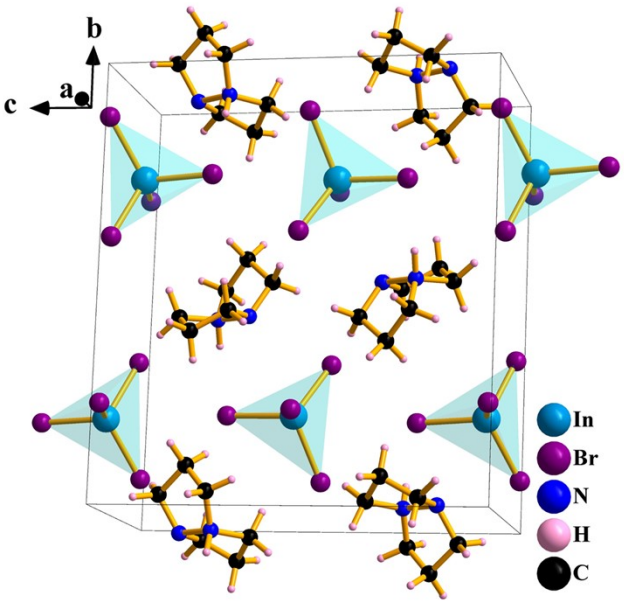

Figure S6. Crystal packing diagram of compound (3.3.0-Dabco)[$InBr_4$] at 200 K.

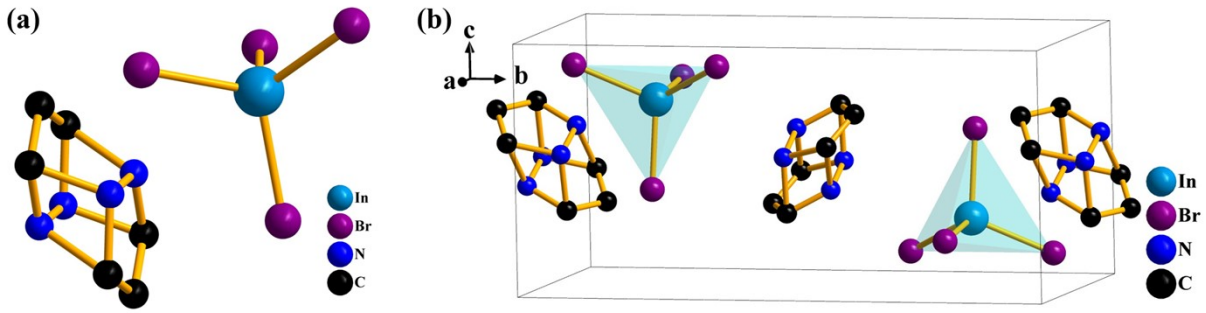

Figure S7. The asymmetric unit (a) and packing diagram (b) of compound (3.3.0-Dabco)[$InBr_4$] at 298 K. The nitrogen atoms are in a highly disordered state, and hydrogen atoms have been omitted for display convenience.

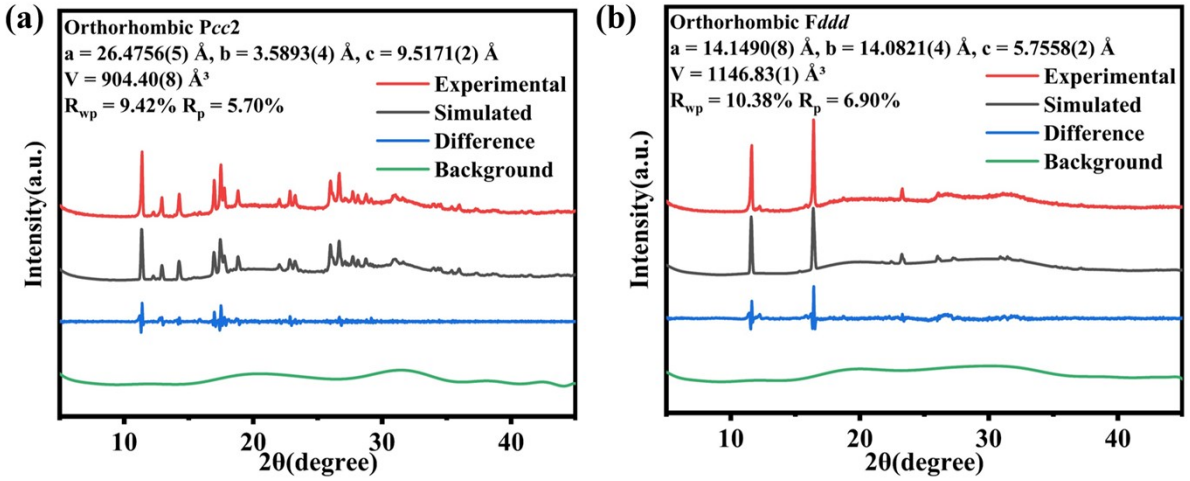

Figure S8. Pawley refinement of PXRD data of compound **1** collected at 343 K (a) and 373 K (b).

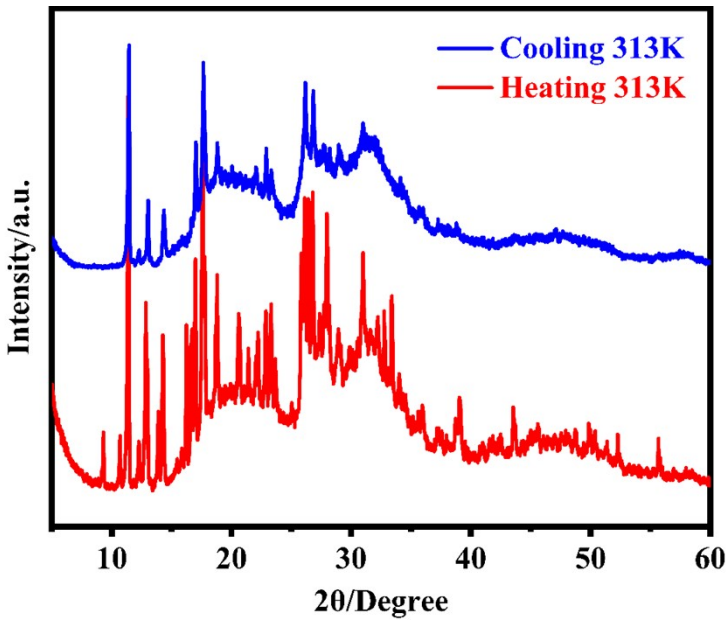

Figure S9. XRD patterns of compound **1** at 343 K during the heating process and at 313 K during the cooling process.

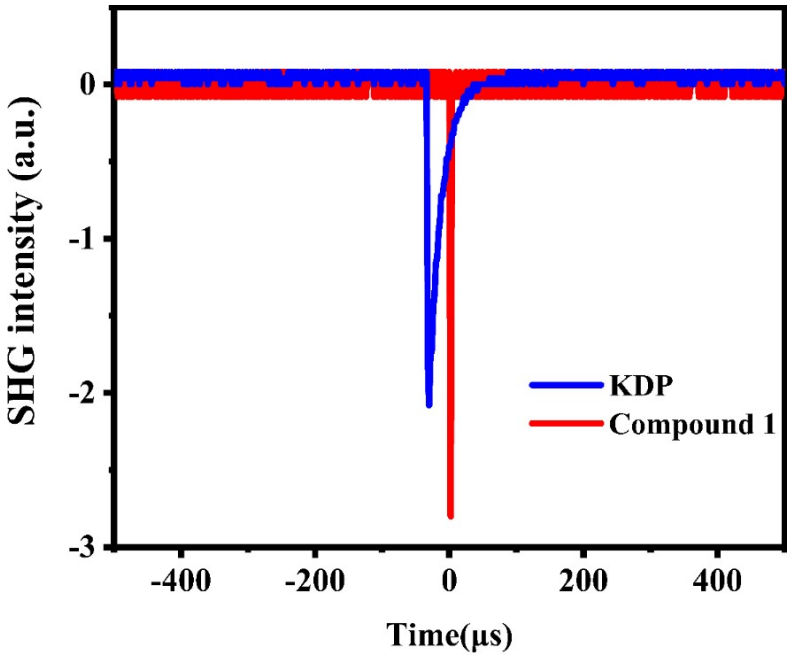

Figure S10. Comparison chart of the SHG signal of compound **1** and KDP at LTP.

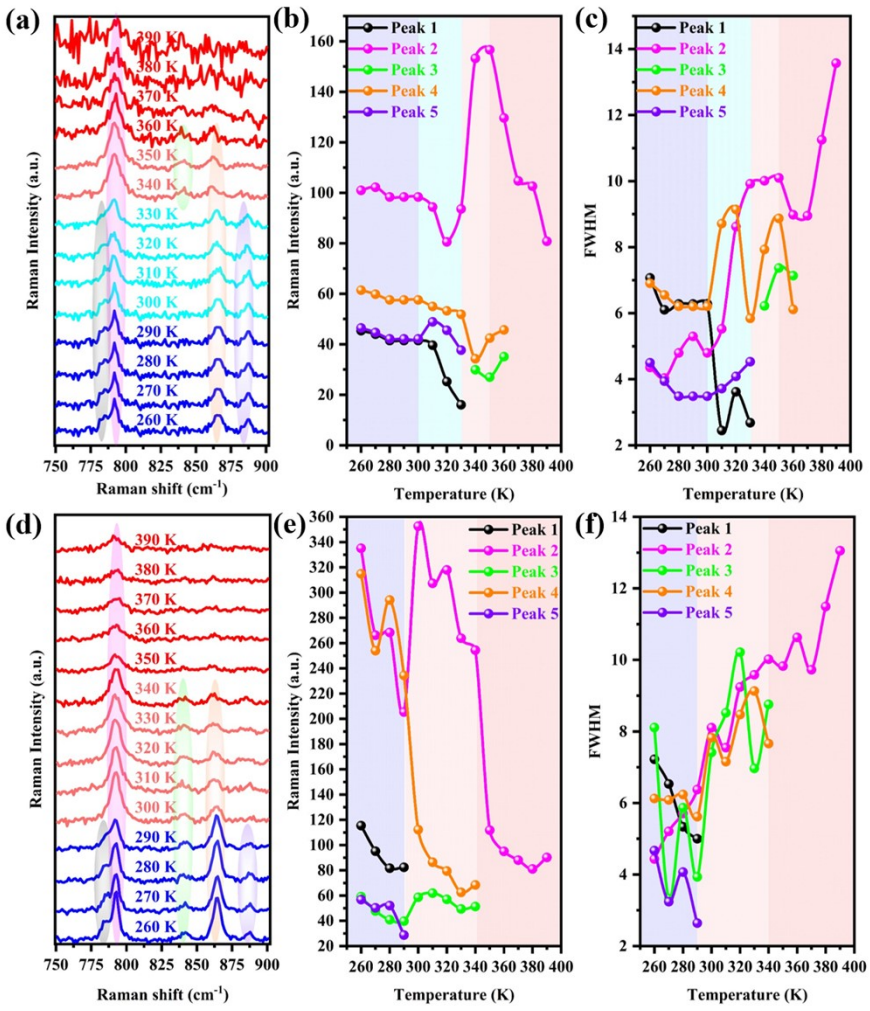

Figure S11. Raman spectra of the characteristic peaks of the N-N bond during the heating process (a), peak intensity (b), and FWHM (c); Raman spectra of the characteristic peaks of the N-N bond during the cooling process (d), peak intensity (e), and FWHM (f).

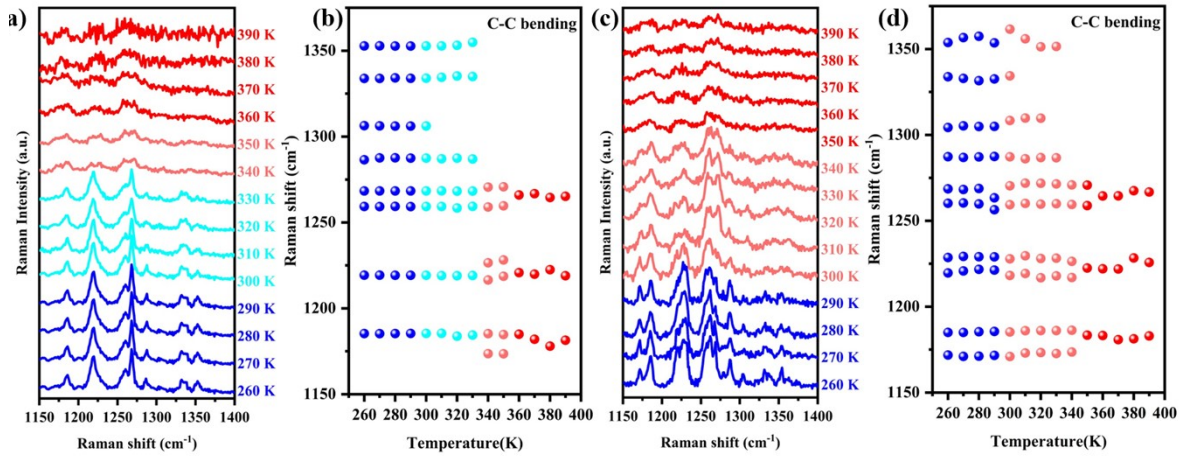

Figure S12. Raman spectra of C-H bond bending vibration of Compound **1** during the heating (a) and cooling (c) processes, and scatter plots of the Raman shift of the characteristic vibrational peaks (1150–1400 cm^{-1}) fitted by the Lorentz function during the heating (b) and cooling (d) processes as a function of temperature.

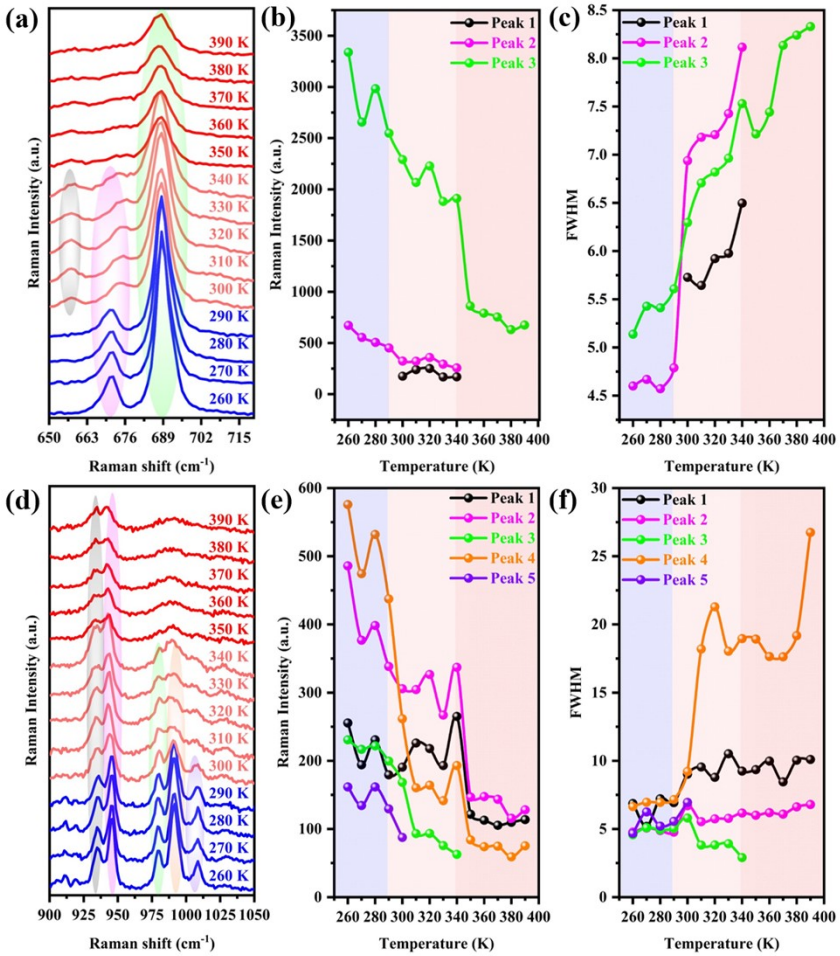

Figure S13. Characteristic peaks of C-Br stretching vibration during the cooling process (a), and the corresponding temperature-dependent peak intensity (b) and FWHM (c); characteristic peaks of five-membered ring breathing vibration (d), and the corresponding temperature-dependent peak intensity (e) and FWHM (f).

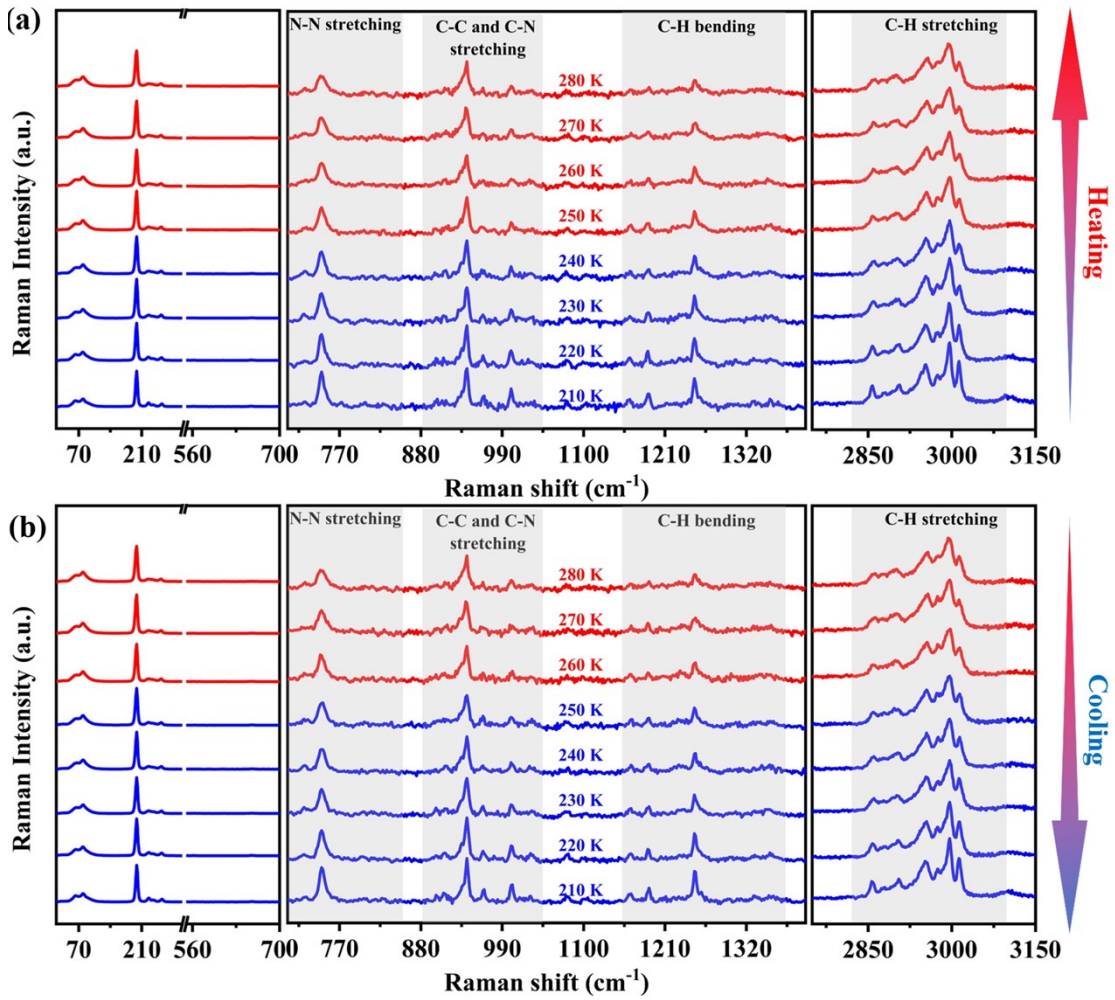

Figure S14. Raman spectra of (3.3.0-Dabco)[$InBr_4$] during the heating process (a) and cooling process (b).

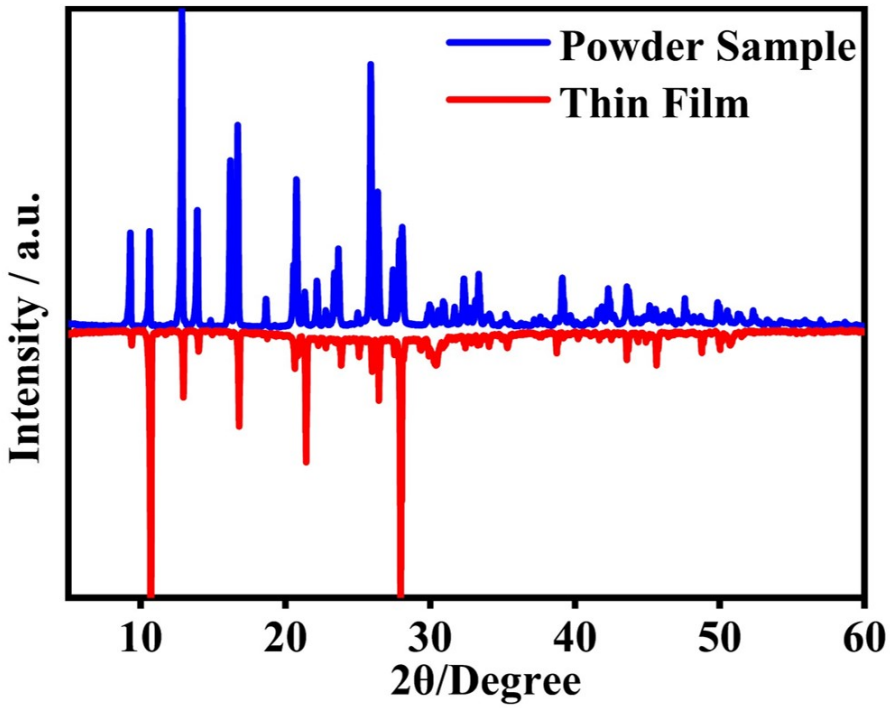

Figure S15. XRD pattern of the thin film sample of Compound **1**

Table S1. The supplier and purity information of all chemical reagents used in the experiments

Chemical Name	CAS Number	Purity	Brand
Hydrobromic acid (HBr)	10035-10-6	⩾ 40.0%	Shanghai Reagent
Hydrazine hydrate ($N_2H_4·H_2O$)	10217-52-4	80%	Adamas
Methyl acrylate ($C_4H_6O_2$)	96-33-3	⩾99%	Adamas
Lithium aluminum hydride ($LiAlH_4$)	16853-85-3	97%	Adamas
Tetrahydrofuran (C_4H_8O)	109-99-9	99.9%	Adamas
Ethanol (C_2H_5OH)	64-17-5	99%	Shanghai Reagent
Dibromomethane (CH_2Br_2)	74-95-3	99%	Adamas
Indium(III) bromide (Br_3In)	13465-09-3	98%	Adamas

Table S2. Crystal data and structure refinements for compounds (3.3.0-Dabco)[$InBr_4$] and **1**.

Empirical formula	$C_6H_{13}Br_4InN_2$		$C_7H_{14}Br_5InN_2$	
Formula weight	547.64	547.64	640.57	640.57
Temperature/K	199.99(10)	298.22(10)	249.95(10)	323.00(10)
Crystal system	monoclinic	monoclinic	orthorhombic	orthorhombic
Space group	$P2_1/c$	$P2_1/m$	$Pna2_1$	$Pn2_1a$
a/Å	6.9893(2)	6.8022(3)	16.5418(5)	16.5863(6)
b/Å	14.9454(4)	15.1280(6)	11.5185(3)	8.6174(4)
c/Å	13.3766(3)	7.0226(3)	8.4636(2)	11.5822(4)
Volume/Å^3	1396.79(6)	722.53(5)	1612.63(7)	1655.46(12)
Z	4	2	4	4
ρ_{calc}g/cm^3	2.604	2.291	2.638	2.570
μ/mm^{-1}	13.100	12.651	13.830	13.473
F(000)	1008.0	442.0	1176.0	1176.0
Crystal size/mm^3	0.01×0.01×0.01	0.01×0.01×0.01	0.02×0.02 × 0.01	0.02×0.02× 0.01
Radiation	Mo Kα (λ = 0.71073)	Mo Kα (λ = 0.71073)	Mo Kα (λ = 0.71073)	Mo Kα (λ = 0.71073)

2θ range for data collection/°	6.094 to 61.592	5.802 to 52.742	5.974 to 52.744	5.892 to 62.048
Index ranges	-10≤h≤9, -20≤k≤21, -18≤l≤18	-8≤h≤8, -18≤k≤18,-8≤l≤8	-19≤h≤20, -12≤k≤14, -10≤l≤10	-22≤h≤22, -11≤k≤11, -16≤l≤15
Reflections collected	30767	8129	16454	20264
Independent reflections	3907 [R_{int}= 0.0533, R_{sigma}= 0.0318]	1536 [R_{int}= 0.0339, R_{sigma}= 0.0237]	3274 [R_{int} = 0.0536, R_{sigma} = 0.0352]	4283 [R_{int} = 0.0395, R_{sigma} = 0.0363]
Data/restraints/parameters	3907/0/122	1536/60/73	3274/152/137	4283/178/219
Goodness-of-fit on F^2	1.063	1.070	1.057	1.003
Final R indexes [I>=2σ (I)]	R_1 = 0.0300, wR_2 = 0.0660	R_1 = 0.0499, wR_2 = 0.1548	R_1 = 0.0297, wR_2 = 0.0682	R_1 = 0.0329, wR_2 = 0.0629
Final R indexes [all data]	R_1 = 0.0441, wR_2 = 0.0694	R_1 = 0.0614, wR_2 = 0.1638	R_1 = 0.0335, wR_2 = 0.0694	R_1 = 0.0723, wR_2 = 0.0732
Largest diff. peak/hole / e $Å^{-3}$	0.74/-1.28	1.09/-1.42	0.71/-0.76	0.53/-0.45
Flack parameter	\	\	-0.006(8)	0.01(2)

Table S3. Selected bond lengths [Å] and bond angles [°] for (3.3.0-Dabco)[$InBr_4$] at 200 K.

Atom	**Atom**	**Length/**[Å]	**Atom**	**Atom**	**Atom**	**Angle/°**
In1	Br2	2.4748(4)	Br2	In1	Br1	115.156(14)
In1	Br1	2.4897(4)	Br2	In1	Br3	111.667(15)
In1	Br3	2.5049(4)	Br2	In1	Br4	107.010(14)
In1	Br4	2.5198(4)	Br1	In1	Br3	105.809(14)
N1	N2	1.487(4)	Br1	In1	Br4	111.426(16)

N1	C4	1.477(4)	Br3	In1	Br4	105.399(13)
N1	C3	1.480(5)	C4	N1	N2	105.0(2)
N2	C1	1.508(6)	C4	N1	C3	114.0(3)
N2	C6	1.492(5)	C3	N1	N2	105.6(3)
C4	C5	1.495(5)	N1	N2	C1	106.9(3)
C3	C2	1.511(5)	N1	N2	C6	107.6(3)
C1	C2	1.493(6)	C6	N2	C1	117.4(3)
C5	C6	1.507(6)	N1	C4	C5	104.5(3)

Table S4. Selected bond lengths [Å] and bond angles [°] for (3.3.0-Dabco)[$InBr_4$] at 298 K.

Atom	**Atom**	**Length/**[Å]	**Atom**	**Atom**	**Atom**	**Angle/°**
In1	Br2	2.4842(9)	Br2	In1	$Br2^1$	112.13(6)
In1	$Br2^1$	2.4843(9)	$Br2^1$	In1	Br3	109.46(4)
In1	Br3	2.4874(16)	Br2	In1	Br3	109.46(4)
In1	Br4	2.5007(16)	$Br2^1$	In1	Br4	107.65(4)
N1	C6	1.52(3)	Br2	In1	Br4	107.65(4)
N1	$N2^2$	1.61(3)	Br3	In1	Br4	110.46(7)
N1	N2	1.55(3)	C6	N1	$N2^2$	65.1(13)
N1	$C4^2$	1.61(3)	C6	N1	N2	102.2(15)
C6	$N2^2$	1.68(3)	C6	N1	$C4^2$	108.3(16)
C6	C5	1.33(3)	N2	N1	$N2^2$	87.4(13)
N2	C4	1.39(3)	$N2^2$	N1	$C4^2$	51.1(12)
C5	C4	1.46(3)	N2	N1	$C4^2$	103.9(16)
In1	Br2	2.4842(9)	N1	C6	$N2^2$	59.9(12)
			C5	C4	$N1^2$	95.6(16)

Table S5. Selected bond lengths [Å] and bond angles [°] for **1** at 250 K.

Atom	**Atom**	**Length/**[Å]	**Atom**	**Atom**	**Atom**	**Angle/°**
In1	Br4	2.4997(13)	Br1	In1	Br4	109.59(3)
In1	Br1	2.4963(13)	Br1	In1	Br3	107.90(5)
In1	Br3	2.4967(8)	Br3	In1	Br4	108.08(5)
In1	Br2	2.4952(9)	Br2	In1	Br4	111.35(5)
Br5	C7	1.927(8)	Br2	In1	Br1	107.85(5)

N1	N2	1.479(7)	Br2	In1	Br3	111.99(3)
N1	C7	1.485(10)	N2	N1	C7	103.1(6)
N1	C6	1.513(11)	N2	N1	C6	108.5(6)
N1	C1	1.510(11)	N2	N1	C1	108.9(6)
N2	C3	1.440(13)	C7	N1	C6	111.7(6)
N2	C4	1.466(13)	C7	N1	C1	110.8(6)
C6	C5	1.5394(14)	C1	N1	C6	113.2(8)
C1	C2	1.5390(14)	C3	N2	N1	107.9(7)
C5	C4	1.5395(14)	C3	N2	C4	113.0(9)
C3	C2	1.5393(14)	C4	N2	N1	107.4(7)
			C1	C2	C3	103.3(8)

Table S6. Selected bond lengths [Å] and bond angles [°] for **1** at 323 K.

Atom	**Atom**	**Length/**[Å]	**Atom**	**Atom**	**Atom**	**Angle/°**
In1	Br2	2.489(3)	Br2	In1	Br3	108.27(13)
In1	Br3	2.4935(7)	Br2	In1	Br4	109.38(3)
In1	Br4	2.496(3)	Br2	In1	Br5	109.31(14)
In1	Br5	2.4910(8)	Br3	In1	Br4	108.00(14)
Br1	C7	1.903(13)	Br5	In1	Br3	112.45(3)
N1	C6	1.515(18)	Br5	In1	Br4	109.38(14)
N1	N2	1.589(15)	C6	N1	N2	107.7(12)
N1	C1	1.356(19)	C6	N1	C7	100.6(13)
N1	C7	1.598(15)	N2	N1	C7	95.1(13)
N1	C1A	1.35(2)	C1	N1	C6	123.3(17)
N1	C7A	1.612(19)	C1	N1	N2	107.4(13)
N1	C6A	1.53(2)	C1	N1	C7	118.8(13)
N1	N2A	1.571(16)	C1A	N1	C7A	125(2)
C3	N2	1.40(3)	C1A	N1	C6A	124(2)
C3	C2	1.66(3)	C1A	N1	N2A	106.5(16)
C4	N2	1.43(3)	C6A	N1	C7A	94.6(17)
C4	C5	1.49(3)	C6A	N1	N2A	106.9(15)
C6	C5	1.54(2)	N2A	N1	C7A	95.5(15)
C2	C1	1.50(2)	N2	C3	C2	104.7(14)

C1A	C2A	1.52(3)	N2	C4	C5	109.0(18)
Br1A	C7A	1.924(18)	N1	C6	C5	99.1(13)
C6A	C5A	1.53(3)	C3	N2	N1	104.0(15)
C5A	C4A	1.46(3)	C3	N2	C4	116.5(18)
C3A	C2A	1.68(3)	C4	N2	N1	102.1(15)
C3A	N2A	1.42(3)	C1	C2	C3	95.6(13)
C4A	N2A	1.41(4)	C4	C5	C6	101.7(16)
			C4A	N2A	C3A	112(2)

Table S7. Point charge model analysis of (3.3.0-Dabco)[$InBr_4$]. According to the crystal structure data at 200 K, we select a unit cell and make an assumption that the positive charge of $[C_6H_{13}N]^+$ and the negative charge of $[InBr_4]^-$ is on the N atomand In atom, respectively.

Atoms	Coordinate		Center coordinate
N	N1 (0.36737, 0.9668, 0.2687)	N2 (0.63260, 1.0332, 0.7313)	(0.5, 0.5, 0.5)
	N3 (0.36737, 0.5332, 0.7687)	N4 (0.63263, 0.4668, 0.2313)	
	N5 (0.3674, -0.0332, 0.2687)	N6 (0.63263, 0.0332, 0.7313)	
In	In1 (0.76447, 0.25348, 0.42382)	In2 (0.23553, 0.75348, 0.07618)	(0.5, 0.5, 0.5)
	In3 (0.76449, 0.24652, -0.07618)	In4 (0.23551, 0.75348, 1.07618)	
	In5 (0.76447, 0.24652, 0.92382)	In6 (0.23553, 0.74652, 0.57618)	

Table S8. Point charge model analysis of Compound **1**. According to the crystal structure data at 250 K, we select a unit cell and make an assumption that the positive charge of $[C_7H_{14}NBr]^+$ and the negative charge of $[InBr_4]^-$ is on the N atomand In atom, respectively.

Atoms	Coordinate		Center coordinate
N	N1 (0.0034, 0.2762, 0.5331)	N2 (0.5034, 0.2238, 0.5331)	(0.5, 0.5, 0.25648)
	N3 (0.9966, 0.7238, 0.0331)	N4 (0.4966, 0.7762, 0.0331)	
In	In1 (0.73187, 0.86494, 0.50648)	In2 (0.76813, 0.36494, 0.00648)	(0.5, 0.5, 0.2831)
	In3 (0.23187, 0.63506, 0.50648)	In4 (0.26813, 0.13506, 0.00648)	

$$P = \lim \frac{1}{V} \Sigma q_i r_i$$

$$= (q_N r_N + q_{In} r_{In}) / V$$

$$= [(e \times 0.2831) + (-e \times 0.25648) \times 4 \times c] / V$$

$$= [(0.02662 \times 1.6 \times 10^{-19} \times 4 \times 8.4636 \times 10^{-10} C \text{g} m] / 1612.63 \times 10^{-30} m^3$$

$$= 0.008952 C \text{g} m^{-2} = 0.895 C \mu \text{g} m^{-2}$$

(1) Sheldrick, G. A short history of SHELX. *Acta Crystallographica Section A* **2008**, *64* (1), 112–122.
(2) Dolomanov, O. V.; Bourhis, L. J.; Gildea, R. J.; Howard, J. A. K.; Puschmann, H. OLEX2: a complete structure solution, refinement and analysis program. *J. Appl. Crystallogr.* **2009**, *42* (2), 339–341.
(3) Sheldrick, G. Crystal structure refinement with SHELXL. *Acta Crystallographica Section C* **2015**, *71* (1), 3–8.